Thermoelectric properties of n-type Bi2Te2.7Se0.3 and p-type Bi0.5Sb1.5Te3 thin films deposited by direct current magnetron sputtering

Daniel Bourgault, C. Giroud Garampon, N. Caillault, L. Carbone, J.A. Aymami

Thermoelectric properties of n-type Bi2Te2.7Se0.3 and p-type Bi0.5Sb1.5Te3 thin films deposited by direct current magnetron sputtering

Daniel Bourgault, C. Giroud Garampon, N. Caillault, L. Carbone, J.A. Aymami

Thermoelectric properties of n-type $Bi_2Te_{2.7}Se_{0.3}$ and p-type $Bi_{0.5}Sb_{1.5}Te_3$ thin films deposited by direct current magnetron sputtering

D. Bourgault [a,b,*], C. Giroud Garampon [a], N. Caillault [a], L. Carbone [a], J.A. Aymami [a]

[a] Schneider-Electric France, 38TEC/T1, 37 quai Paul Louis Merlin, 38050 Grenoble Cedex 9, France
[b] Institut Néel/Centre National de la Recherche Scientifique, 25 Avenue des Martyrs, BP 166, 38042 Grenoble Cedex 9, France

ARTICLE INFO

Article history:
Received 23 March 2007
Received in revised form 20 May 2008
Accepted 3 June 2008
Available online xxxx

Keywords:
Thermoelectric effect of thin films (73.50Lw)
Deposition methods of thin films (81.15.-z)
Electrical conductivity of thin films (73.50.-h)
Thermoelectric properties
Thin film
Magnetron sputtering
Electrical conductivity
X-ray diffraction

ABSTRACT

n-type and p-type thermoelectric thin films have been deposited by direct current magnetron sputtering from n-type $Bi_2Te_{2.7}Se_{0.3}$ and p-type $Bi_{0.5}Sb_{1.5}Te_3$ targets on glass and Al_2O_3 substrates. X-ray diffraction and energy dispersive spectrometry combined with electrical measurements such as Seebeck coefficient and electrical resistivity were used for the thermoelectric thin films characterization. It was found that the composition of the sputtered thin films was close to the sputtering target stoichiometry for the tested deposition conditions and that the thin film composition did not seem to be the determinant parameter for the thermoelectrical properties. Indeed, the chamber pressure and plasma power have a greater influence on the thermoelectrical performances of the films. Annealing in Ar atmosphere (250 °C for n-type and 300 °C for p-type films) enhanced the film crystallization and yield power factors higher than 1 mW/K^2 m.

1. Introduction

Most applications of thermoelectricity deal with cooling and power generation, both based on thermal and electrical energy conversion. The thermoelectrical properties of bismuth telluride compounds at room temperature are already used for the fabrication of micro cooler devices [1–3].

However, sizing and integration problems of new devices cannot be solved with existing bulk materials: Thermoelectric thin film development is necessary. The thermoelectric properties of thin films have long been of small interest compared to those of bulk materials. They have been only recently improved with Bi_2Te_3–Sb_2Te_3 super lattices for which a high performance increase has been obtained due to the dimensionality reduction [4].

Thermoelectrical thin films have already been prepared by different deposition techniques such as thermal co-evaporation [5,6], flash evaporation [7], radio frequency sputtering [8], ion beam sputtering [9], molecular beam epitaxy [10,11], hot wall epitaxy [12,13], electrochemical deposition [14,15], Metal Organic Chemical Vapor Deposition (MOCVD) [16] or pulsed laser deposition [17,18].

The aim of this work was to deposit bismuth telluride thin films by direct current (dc) magnetron sputtering using one single target and to optimize the thermoelectrical properties. According to previous research on $Bi_2Te_{3-y}Se_y$ and $Bi_{2-x}Sb_xTe_3$ thin film systems [19–23], the target compositions were chosen as follows: $Bi_2Te_{2.7}Se_{0.3}$ for n-type and $Bi_{0.5}Sb_{1.5}Te_3$ for p-type thermoelectric films. Two types of substrates were used: glass microscope slides and polycrystalline Al_2O_3. Film composition and thermoelectric performances were investigated before and after Ar annealing.

2. Experimental details

2.1. Film deposition

Films were deposited at room temperature using a dc magnetron sputtering device. Commercial 50 mm diameter hot pressed targets were used with the following composition: $Bi_2Te_{2.7}Se_{0.3}$ for n-type and $Bi_{0.5}Sb_{1.5}Te_3$ for p-type materials. The stoichiometry of both targets was verified by Energy Dispersive X-ray Spectroscopy (EDS) with a ±3% accuracy. Both glass microscope slides and polycrystalline Al_2O_3 were used as substrates, with 25×25 mm^2 dimension. The substrates were cleaned using deionized water prior to a 15 min alcohol ultrasonic bath.

Pressure before deposition was lower than $5\cdot10^{-4}$ Pa. A 10 min target pre-sputtering was used to eliminate surface contamination prior to plasma deposition. The sputtering conditions and the resulting film thicknesses are described in Table 1.

After deposition, films were annealed in Ar atmosphere at different temperatures (up to 250 °C and 300 °C for respectively $Bi_2Te_{2.7}Se_{0.3}$ and $Bi_{0.5}Sb_{1.5}Te_3$ films) and for different durations (up to 32 h).

* Corresponding author. Schneider-Electric France, 38TEC/T1, 37 quai Paul Louis Merlin, 38050 Grenoble Cedex 9, France. Tel.: +33 4 76 39 13 49; fax: +33 4 57 78 62.
E-mail address: daniel.bourgault@grenoble.cnrs.fr (D. Bourgault).

Please cite this article as: D. Bourgault, et al., Thin Solid Films (2008), doi:10.1016/j.tsf.2008.06.001

Table 1
Sputtering parameters and thicknesses of n-type BiTeSe thin films with $Bi_2Te_{2.7}Se_{0.3}$ nominal composition deposited on glass and Al_2O_3 substrates

Sample name	Substrate type	Target/substrate distance (cm)	Plasma power (W)	Argon pressure (Pa)	Deposition time (mn)	Film thickness (nm)	Remarks
Th23	Glass	6	4	$4\cdot10^{-2}$	60	730	
Th27				7	30	100	Not analyzed in composition
Th31			15	$4\cdot10^{-2}$	30	1450	
Th33				7	60	1100	
Th35		3	4	$4\cdot10^{-2}$	30	910	
Th39				7	60	590	
Th41			15	$4\cdot10^{-2}$	60	8700	Not measurable after annealing
Th43				7	30	2200	
Th24	Al_2O_3	6	4	$4\cdot10^{-2}$	60	750	
Th28				7	30	100	Not analyzed in composition
Th32			15	$4\cdot10^{-2}$	30	1600	
Th34				7	60	1150	
Th36		3	4	$4\cdot10^{-2}$	30	980	
Th40				7	60	620	
Th42			15	$4\cdot10^{-2}$	60	7500	Not measurable after annealing
Th44				7	30	1500	

2.2. Film characterization

Film thickness was measured using a stylus surface profiler (Dektak 3.0).

Film crystallization was investigated with an X-ray Diffraction (XRD) system (D5000 Brucker) in the conventional Θ–2Θ mode using the Cu Kα radiation. EDS was performed on an environmental scanning electron microscope (ESEM FEI Quanta 200) operating at 18 kV for the films composition determination. At least three different regions of each sample were analyzed with the same conditions (accelerating voltage, beam current, magnification, acquisition time). Quantitative analysis of the different elements (atomic percent concentration) was performed by non-standard analysis (using ZAF correction procedures) with a ±3% accuracy.

The Seebeck coefficient S (μV/K) and the electrical resistivity ρ (mΩ cm) were measured at room temperature to determine the power factor $P=S^2/\rho$. This factor gives an indication of the thermoelectric performance, usually expressed by the figure of merit $Z=S^2/\rho\kappa=P/\kappa$ (κ being the thermal conductivity).

A device was developed (see Fig. 1) to measure the Seebeck coefficient of the films by applying a thermal gradient along the film plane.

The left part of the device (hot zone) was regulated using a heating cartridge and the right part of the device (cool zone) was maintained at 17 °C with flowing water.

A mechanical pressure ensured the thermal and electrical contacts quality at the hot and cold ends of the set-up. The temperature gradient was measured with an accuracy of ±1 °C by two K-type thermocouples (0.1 mm diameter) located at the surface of the films. The induced voltage was measured using an Agilent 34401A Digital multimeter. The estimated accuracy of the Seebeck coefficient measurement was ±5%. The homogeneity of the Seebeck value along the films was verified by changing the probe distances. In addition, different thermal gradients with a maximum of $\Delta T=20$ °C yield a constant Seebeck coefficient.

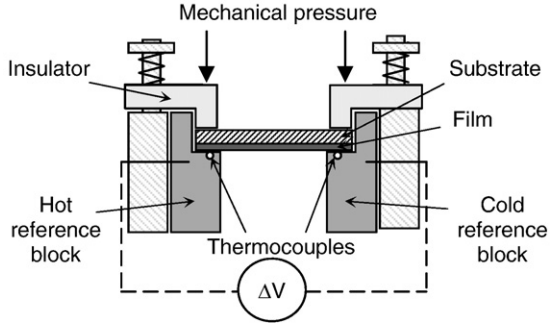

Fig. 1. Schematic of experimental set-up for Seebeck coefficient measurement.

Electrical resistivity was measured at room temperature using the standard four-points probe measurement. The universal Jandel four linear points test equipment associated to a Keithley 237 current source and a Keithley 199 multimeter yielded resistivity measurements with an accuracy of ±5%. According to the different accuracy estimations, the power factor is calculated with an accuracy of ±15%.

3. Results and discussion

3.1. n-type $Bi_2Te_{2.7}Se_{0.3}$ thermoelectric thin films

3.1.1. Electrical properties and composition of as grown films

Electrical properties of as grown n-type films sputtered on glass substrates from the $Bi_2Te_{2.7}Se_{0.3}$ target are summarized in Table 2. Power factors were calculated from the S and ρ measurements of the different films. Deposition conditions and EDS composition analysis are also reported in this table. The samples are sorted by growing power factor.

Results on as grown films are as follows:

- low Ar deposition pressure yields low resistivity and consequently high power factor.
- low Se contents (<6 at.%) lead to low power factor values. The low thermoelectrical properties of sample Th43 are however not yet understood.

The first point shows that the sputtering mechanism rather impacts the electrical resistivity than the Seebeck coefficient.

Even though the power factor values are very low due to unannealing, it can be noticed that a deposition parameter such as pressure has a strong influence on the electrical resistivity. Indeed, it is known that a high pressure reduces the mean free path and consequently the particles having a lower energy change the nucleation and the growth mechanisms at the substrate surface.

Table 2
Seebeck coefficient (S), resistivity (ρ) and power factor (P) of n-type BiTeSe thin films with $Bi_2Te_{2.7}Se_{0.3}$ nominal composition deposited on glass substrates

Sample name	Argon pressure (Pa)	Composition (at.%) ±3%	S (μV/K) ±5%	ρ (mΩ cm) ±5%	P (mW/K² m) ±15%
Th33	7	$Bi_{37.2}$ Te_{6} [illegible]	−110	23.4	0.052
Th43	7	$Bi_{35.2}$ $Te_{58.1}$ $Se_{6.7}$	−196	68.7	0.056
Th27	7	Not analysed	−133	20.8	0.085
Th39	7	$Bi_{35.9}$ $Te_{60.1}$ $Se_{4.0}$	−157	23.3	0.11
Th23	$4\cdot10^{-2}$	$Bi_{35.0}$ $Te_{58.0}$ $Se_{7.0}$	−201	34.0	0.12
Th35	$4\cdot10^{-2}$	$Bi_{38.8}$ $Te_{54.7}$ $Se_{6.5}$	−108	5.3	0.22
Th31	$4\cdot10^{-2}$	$Bi_{35.7}$ $Te_{57.0}$ $Se_{7.3}$	−108	5.1	0.23
Th41	$4\cdot10^{-2}$	$Bi_{42.1}$ $Te_{51.1}$ $Se_{6.8}$	−77	2.4	0.24

Ar deposition pressure and composition determined by EDS analysis are also reported.

Please cite this article as: D. Bourgault, et al., Thin Solid Films (2008), doi:10.1016/j.tsf.2008.06.001

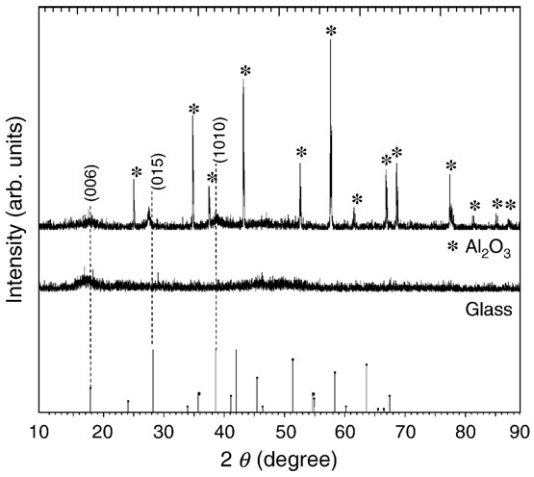

Fig. 2. XRD pattern of n-type BiTeSe thin films with $Bi_2Te_{2.7}Se_{0.3}$ nominal composition deposited on glass and Al_2O_3 substrates before annealing. Deposition conditions: target-to-substrate distance: 6 cm; plasma power: 4 W; Ar pressure: 0.04 Pa; deposition time: 60 min. Symbols (*) correspond to Al_2O_3 peaks. JCPDS Card 050-0954 of the $Bi_2Te_{2.7}Se_{0.3}$ phase is also reported.

The large resistivity values attributed to this low activation energy (thus inefficient growth) also correspond to low Se contents. High deposition pressure conditions rather influence the yield of Se particles (low atomic percent) than Bi or Te elements for which a small composition variation (less than 13%) from the initial target stoichiometry is obtained whatever the deposition conditions.

3.1.2. Initial crystallization of the sputtered films

Fig. 2 shows typical XRD patterns of thin films sputtered on glass (Th23) and Al_2O_3 (Th24) substrates. Compared to the power diffraction file (Card 050-0954) [24], the patterns of both samples can be attributed to the $Bi_2Te_{2.7}Se_{0.3}$ phase. For sample Th24 the clearest peaks of the $Bi_2Te_{2.7}Se_{0.3}$ phase corresponds to the (015) plane but the intensity is very low compared to the Al_2O_3 substrate peaks. The same phase is found in sample Th23 but with a preferred orientation since only a small (006) peak appears in the pattern.

The very low peak intensities of the $Bi_2Te_{2.7}Se_{0.3}$ phase are attributed to the low film crystallization. This explains why the power factors of the as-deposited films are low compared to other results in the literature [25,26]. As described in further sections of this work, annealing of these films will significantly improve thermoelectric performance.

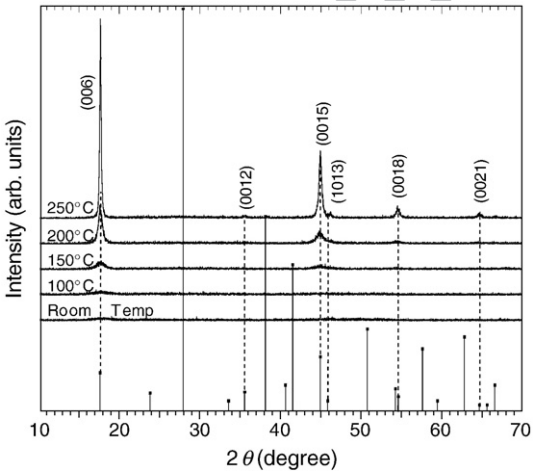

Fig. 3. XRD patterns of n-type BiTeSe thin films with $Bi_2Te_{2.7}Se_{0.3}$ nominal composition deposited on glass substrates after annealing at temperatures ranging from room temperature to 250 °C. Same deposition conditions than samples presented in Fig. 2. JCPDS Card 050-0954 of the $Bi_2Te_{2.7}Se_{0.3}$ phase is also reported.

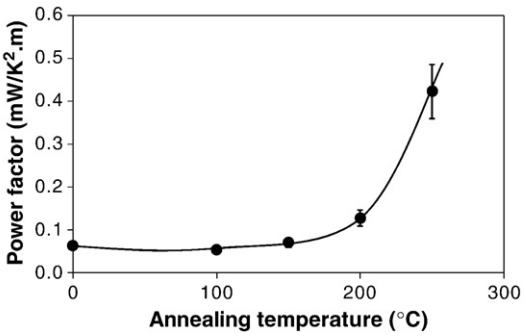

Fig. 4. Power factor versus annealing temperature for an n-type BiTeSe thin film with $Bi_2Te_{2.7}Se_{0.3}$ nominal composition deposited on glass substrate. Same deposition conditions than samples presented in Fig. 2; annealing time: 120 min.

3.1.3. Annealing temperature effect on film crystallization

The sputtered films were annealed in order to improve crystallization and thermoelectrical performances according to previous studies [27–29]. The glass sputtered sample Th23 was annealed with different annealing temperatures during a constant time of 2 h. Fig. 3 shows the power factor increase for an annealing temperature ranging from 20 °C up to 250 °C.

The power factor reaches 0.4 mW/K² m (S=150 μV/K and ρ=5.3 mΩ cm) for annealing conditions of 2 h at 250 °C. This value is explained by a large decrease of the resistivity due to film crystallization during annealing, as shown in Fig. 4. The $Bi_2Te_{2.7}Se_{0.3}$ pattern (JCPDS Card no 050-0954) [24] reported on this figure confirms that the compound formed is very close to the $Bi_2Te_{2.7}Se_{0.3}$ phase.

Preferred orientation of sample Th23 after annealing is confirmed since only (00l) peaks are found in the XRD patterns. The growth along the c-axis is reproducible as already observed by Giani et al. on epitaxial film of Bi_2Te_3 and Sb_2Te_3 grown by MOCVD on Pyrex and silicon substrates [30].

Quantitative thin film composition after annealing was also analyzed and the film stoichiometry was conserved up to 250 °C.

3.1.4. Annealing duration effect on film crystallization

The optimal temperature of 250 °C obtained on sample Th23 was then used to anneal all samples of Table 1 for different durations.

Fig. 5 shows the corresponding power factor variations for the film sputtered on glass substrate.

The annealing time at 250 °C was increased up to 32 h and Fig. 5 shows that the power factor exceeds 1 mW/K² m. This value can be compared to the best obtained on thin films (3–5 mW/K² m) [25,26] and can be improved by further deposition and annealing conditions optimization.

Fig. 5 also shows two populations of thermoelectric performances corresponding to two different thin films groups.

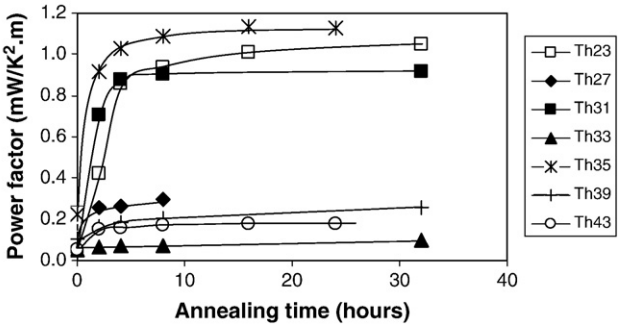

Fig. 5. Power factors versus annealing time for n-type BiTeSe thin films $Bi_2Te_{2.7}Se_{0.3}$ deposited on glass substrates and annealed at 250 °C.

Please cite this article as: D. Bourgault, et al., Thin Solid Films (2008), doi:10.1016/j.tsf.2008.06.001

A first group of samples (Th23, Th31, Th35) deposited at low Ar pressure ($4 \cdot 10^{-2}$ Pa) yielding high power factors, and a second group of samples (Th27, Th33, Th39 and Th43) deposited at higher Ar pressure (7 Pa) yielding lower power factors.

Sample Th41 could not be measured after annealing because of film detachment from the substrate due to high stress across the film thickness (8700 nm). However the as-deposited power factor value was comparable of those of the first sample group.

This confirms the major role of the Ar deposition pressure during sputtering. A complete study with a continuous variation of the deposition pressure showed an optimum for which the highest power factor value is obtained. This work confirmed that the deposition pressure had a strong influence on the grain size after annealing. Grain dimension was enhanced by low deposition pressure leading to large carrier mobility and low resistivity of the samples. This grain growth during annealing highly depends on the nuclei formation during the sputtering step. A recent Atomic Force Microscopy study confirmed this hypothesis: large grains were obtained on annealed samples prepared at low Ar pressure.

Furthermore, it appears within each group of samples that the plasma power is the second most influent deposition parameter. Indeed, both high and low power factor populations show better performances when the power of the plasma is low.

It should also be mentioned that thermoelectrical performance not only depends on the film crystalline quality. As an example, sample Th23 shows the highest *c*-axis alignment (only 00l peaks) but not the highest power factor value.

The use of glass substrate clearly shows that thermoelectric performance of the thin films is not directly correlated to a preferential growth direction.

The same type of study was realized on Al_2O_3 sputtered thin films: the behavior is very similar to that obtained on glass substrate.

Fig. 6 also shows power factor enhancement with annealing duration at 250 °C for these samples (despite of a small decrease after 8 h which we did not investigate yet).

The same two sub-populations can be identified according to Ar pressure and plasma power sputtering conditions and the best power factor value obtained reaches 1 mW/K^2 m.

With this study realized on both glass and Al_2O_3 substrates, we can conclude that thermoelectrical performance does not depend on the substrate type. Indeed, amorphous or polycrystalline substrates lead to the same film morphology (as observed by SEM) and to the same power factor values.

3.2. p-type $Bi_{0.5}Sb_{1.5}Te_3$ thermoelectric thin films

Sputtering conditions and thermal treatments were also investigated on p-type thermoelectric thin films deposited on glass and Al_2O_3 substrates. $Bi_{0.5}Sb_{1.5}Te_3$ is the optimal stoichiometry for the thermoelectric properties.

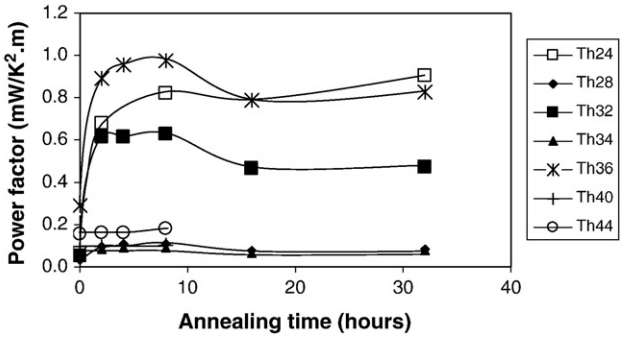

Fig. 6. Power factors versus annealing time for n-type BiTeSe thin films $Bi_2Te_{2.7}Se_{0.3}$ deposited on Al_2O_3 substrates and annealed at 250 °C.

Table 3
Effect of annealing at 300 °C on Seebeck coefficient (S), resistivity (ρ) and power factor (P) for p-type BiSbTe thin films with $Bi_{0.5}Sb_{1.5}Te_3$ nominal composition

Sample	Substrate	Thickness (nm)	Annealing conditions	S (μV/K) ±5%	ρ (mΩ cm) ±5%	P (mW/K^2 m) ±15%
Th54	Glass	700	None	+304	450	$2.6 \cdot 10^{-2}$
			16 h at 300 °C	+191	2.2	1.6
Th59	Al_2O_3	850	None	+154	370	$6.4 \cdot 10^{-3}$
			16 h at 300 °C	+218	2.4	2.0

The influence of sputtering parameters on the thermoelectrical performances of p-type samples are not related here. The following sputtering conditions were chosen: a target-to-substrate distance of 5 cm, a plasma power of 15 W, an Ar pressure of $4 \cdot 10^{-2}$ Pa and a sputtering time of 7 min.

Several unannealed thin films yielded power factors around $2 \cdot 10^{-2}$ mW/K^2 m, lower than literature values [26,29]. The Seebeck coefficient is high (close to 300 μV), but the resistivity is also very high ($5 \cdot 10^{-1}$ Ω cm) due to poor crystallization, as confirmed by XRD analysis.

In a similar way to the n-type films study, p-type films were annealed in order to enhance thermoelectrical performances. As shown by Takashiri et al. in $Bi_{0.4}Sb_{1.6}Te_3$ thin film prepared from nanoparticles [31], the deviation of the atomic composition from stoichiometry is slight for annealing temperatures up to 340 °C.

The p-type thin films were therefore annealed during 16 h at 300 °C to avoid a loss of Te (and consequently an increase in the charge carriers concentration).

Table 3 summarizes the thermoelectric properties obtained before and after annealing of p-type thin films deposited on glass and Al_2O_3 substrates.

On glass substrate, a strong decrease of the resistivity was observed after annealing leading to an increase of the power factor despite a small decrease of the Seebeck coefficient.

The highest power factor value reaches 2.0 mW/K^2 m, which is slightly less than values obtained by other groups [26,32] (~5 mW/K^2 m). Such results are very encouraging since the sputtering conditions were deliberately not optimized here.

Similarly to n-type films, XRD confirms films crystallization after annealing on both types of substrates: glass and Al_2O_3. Here again, thermoelectrical performances could not be correlated to any preferential crystal growth direction.

4. Conclusion

We showed that dc magnetron sputtering process leads to bismuth telluride thin films with a stoichiometry very close to the starting target composition, in contrast to what it is usually claimed in the literature. This point has been verified with the n-type $Bi_2Te_{2.7}Se_{0.3}$ thin films in particular for a low Ar deposition pressure. The stoichiometry is even conserved after an Ar annealing, necessary for phase crystallization enhancement so as to increase thermoelectric properties. However, there is no influence of the substrate type: thermoelectric performance of both n-type and p-type films are similar when sputtered on either glass or Al_2O_3 substrates.

Thermoelectric thin films with acceptable performances have thereby been obtained. For n-type and p-type films, power factors of respectively 1.2 mW/K^2 m and 2.0 mW/K^2 m have been achieved.

Ar deposition pressure and plasma power seem to be the most influent sputtering parameters on thermoelectrical performances.

Sputtering process optimization for further power factor enhancement is currently under study and will soon be related. dc magnetron sputtering process can also be used to develop devices based on n–p pairs in various geometrical configurations. Configurations parallel and perpendicular to the substrate are under investigation.

Please cite this article as: D. Bourgault, et al., Thin Solid Films (2008), doi:10.1016/j.tsf.2008.06.001

Acknowledgements

We thank V. Guenego and D. Charlon for EDS analysis.

References

[1] J. Bierschenk, D.A. Johnson, Electron. Cool. 11 (2005) 24.
[2] H. Böttner, Proceedings of the 24th International Conference on Thermoelectrics, Clemson, USA, June 19–23, 2005, p. 1.
[3] V. Semenyuk, Proceedings of the 25th International Conference on Thermoelectrics, Vienna, Austria, August 6–10, 2006, p. 322.
[4] R. Venkatasubramanian, E. Sivola, T. Colpitts, B. O'Quinn, Nature 413 (2001) 597.
[5] L.W. da Silva, M. Kaviany, A. DeHennis, J.S. Dyck, Proceedings of the 22nd International Conference on Thermoelectricity, La Grande Motte, France, August 17–21, 2003, p. 665.
[6] H. Zou, D.M. Rowe, S.G.K. Williams, Thin Solid Films 408 (2002) 270.
[7] F. Völklein, V. Baier, U. Dillner, E. Kessler, Thin Solid Films 187 (1990) 253.
[8] D. Kim, E. Byon, G-H. Lee, S. Cho, Thin Solid Films 510 (2006) 148.
[9] H. Noro, K. Sato, H. Kagechika, J. Appl. Phys. 73 (1993) 1252.
[10] A. Mzerd, D. Sayah, J.C. Tedenac, A. Boyer, J. Mater. Sci. Lett. 13 (1994) 301.
[11] A. Boyer, E. Cisse, Mater. Sci. Eng. B 13 (1992) 103.
[12] A. Lopez-Otero, Thin Solid Films 49 (1978) 1.
[13] M. Ferhat, B. Liautard, G. Brun, J.C. Tedenac, M. Nouaoura, L. Lassabatere, J. Cryst. Growth, 167 (1996) 122.
[14] J.R. Lim, G.J. Snyder, C.K. Huang, J.A. Herman, M.A. Ryan, J.P. Fleurial, Proceedings of the 21st International Conference on Thermoelectricity, Long Beach CA, USA, August 25–29, 2002, p. 535.
[15] D. Del Fari, S. Diliberto, C. Boulanger, J.M. Lecuire, J. Phys. IV 122 (2004) 53.
[16] A. Giani, F. Pascal-Delannoy, A. Boyer, A. Foucaran, M. Gschwind, P. Ancey, Thin Solid Films 303 (1997) 817.
[17] R.S. Makala, K. Jagannadham, B.C. Sales, H. Wang, Mater. Res. Soc. Symp. Proc. 691 (2002) G8.4.
[18] A. Dauscher, A. Thomy, H. Scherrer, Thin Solid Films 280 (1996) 61.
[19] S.B. Atakulov, U.A. Gafurov, S.A. Kaz'min, Sov. Phys. Semiconduct. 21 (1987) 342.
[20] N.S. Lidorenko, V.N. Kolomoets, Sov. Phys. Dokl. 20 (1976) 699.
[21] Y. Kim, A. DiVenere, G.K.L. Wong, J.B. Ketterson, S. Cho, J.R. Meyer, J. Appl. Phys. 91 (2002) 715.
[22] S. Cho, Y. Kim, J.B. Ketterson, Appl. Phys. A 79 (2004) 1729.
[23] A. Fouracan, A. Sackda, A. Giani, F. Pascal-Delannoy, A. Boyer, Mater. Sci. Eng. B 52 (1998) 154.
[24] JCPDS Data base, Intern. Center for Diffract. Data, PDF2 (Release 2005) Newtown Square, Pennsylvania, USA.
[25] A. Giani, F. Mailly, W. Al Khalfioui, A. Foucaran, A. Boyer, Mater. Sci. Eng. B 107 (2004) 94.
[26] M. Stordeur, G. Willers, Proceedings of 8th European Workshop on Thermoelectrics of European Thermoelectric Society, Kraków, Poland, September 15–17, 2004.
[27] Y.Z. Boikov, B.M. Goltsman, V.A. Kusatov, Sov. Phys. Solid State 20 (1978) 757.
[28] V.D. Das, P.G. Ganesan, Semicond. Sci. Technol. 12 (1997) 195.
[29] D. Kim, G-H. Lee, Mater. Sci. Eng. B 131 (2006) 106.
[30] A. Giani, F. Boulouz, A. Pascal-Delannoy, E. Fouracan, E. Charles, A. Boyer, Mater. Sci. Eng., B 64 (1999) 19.
[31] M. Takashiri, T. Shirakawa, K. Miyazaki, H. Tsukamoto, J. Alloys Comp. 441 (2007) 246.
[32] M. Stolzer, V. Bechstein, J. Meusel, Proceedings of the 16th International Conference on Thermoelectrics, Dresden, Germany, 9, 1997, p. 3, August 26–29.

Please cite this article as: D. Bourgault, et al., Thin Solid Films (2008), doi:10.1016/j.tsf.2008.06.001